Electronic Supplementary Information for

Controllable Electrostatic Manipulation of Structure Building Blocks in Noble Metal Aerogels

Wei Wei,[a,b] René Hübner,[c] Maximilian Georgi,[a] Cui Wang,[a] Xiaodong Wu[d] and Alexander Eychmüller[a]*

[a]Physical Chemistry, Technische Universität Dresden, Andreas-Schubert-Bau, Zellescher Weg 19, 01069 Dresden, Germany.

[b] Center of Analysis and Test, School of Chemistry and Chemical Engineering, Jiangsu University, Xuefu Road 301, 212013 Zhenjiang, China.

[c]Helmholtz-Zentrum Dresden-Rossendorf, Institute of Ion Beam Physics and Materials Research, Bautzner Landstrasse 400, 01328 Dresden, Germany.

[d]College of Materials Science and Engineering, Nanjing Tech University, Puzhu South Road 30, 210009 Nanjing, China.

***E-mail**: alexander.eychmueller@ tu-dresden.de (A.E.)

Experimental Procedures

Reagents and Materials

Chemical reagents including hydrogen tetrachloroaurate (III) ($HAuCl_4 \cdot 3H_2O$), potassium tetrachloropalladate (II) (K_2PdCl_4), cetyltrimethylammonium bromide (CTAB), cetyltrimethylammonium chloride solution (CTAC, 25 wt. % in H_2O), cysteamine (Cys, ≥98.0%), cysteamine hydrochloride (Cys.HCl), L-cysteine hydrochloride (L-Cys.HCl), poly(diallyldimethylammonium chloride) solution (PDDA, 20 wt. % in H_2O), trisodium citrate (NaCA), 3-aminopropionic acid (β-Ala), sodium deoxycholate (NaDC), polyvinylpyrrolidone (PVP, K30), poly(sodium-4-styrenesulfonate) (PSS, Mw = 70000), dopamine hydrochloride (Dop), ascorbate acid (VC), sodium ascorbate (NaVC), and sodium borohydride ($NaBH_4$) were purchased from Sigma-Aldrich or Alfa-Aesar. All reagents were used without further purification. Milli-Q water was used throughout for preparing aqueous solution.

Preparation of Gold Hydrogels

Gold hydrogels were synthesized by an electrostatic-interaction-induced gelation method.

Ligand aqueous solution (400.0 mM, 25.0 μL) and $HAuCl_4 \cdot 3H_2O$ (32.5 mM, 30.8 μL) were added successively in deionized water (4.92 mL) and stirred for *ca.* 5 min. Then, freshly prepared $NaBH_4$ aqueous solution (200.0 mM, 20.0 μL) was rapidly injected, followed by stirring for *ca.* 2 min. The molar ratio of the metal salt (M), ligand (L), and reductant (R) was fixed at 1/10/4. The as-prepared gold nanoparticle solution was further mixed for 10 min.

The colloidal gold hydrogels were formed by rapidly mixing positively charged and negatively charged gold nanoparticle solutions in equal volume ratio. For example, NaCA-ligand-protected gold nanoparticles (0.2 mM, 3 mL) were added into the as-prepared CTAB-ligand-protected gold nanoparticles (0.2 mM, 3 mL) followed by stirring for *ca.* 2 min (~ 400 rpm) to accelerate the gelation process. Finally, the formed aggregates were assembled to yield Au-hydrogels by leaving it without further moving. Different structural units can be obtained by adjusting the volumes of the two gold nanoparticle solutions.

For scale-up production, aqueous solutions of the ligand (400.0 mM, 5 mL) and $HAuCl_4 \cdot 3H_2O$ (32.5 mM, 6.15 mL) were added in 385 mL deionized water and stirred for ca. 5 min. Then, freshly prepared $NaBH_4$ aqueous solution (200.0 mM, 4 mL) was rapidly injected in the above mixture, followed by stirring for ca. 20 s and grounding > 20 min. The hydrogels were prepared by mixing two different ligand-protected gold NP solutions (each 400 mL).

Preparation of Bimetallic Hydrogels

Bimetallic hydrogels were synthesized by a one-step approach of mixing positively charged and negatively charged noble metal particle solutions. The synthesis process is the same as

that for the gold hydrogels, except that two metal precursor salts were introduced. The molar ratio of the different metal precursor salts was set to 1:1 for the bimetallic systems, and the total concentration of the metal salts in the final solution, if not specified, was fixed at 0.5 mM. Different structural units can be obtained by adjusting the volumes of the two noble metal nanoparticle solutions. For the dopamine-induced gelation process, the dopamine/gold ratio was fixed at 2.5/1 (Solubility); the proportions of the other precursors were the same as for the electrostatic-interaction-induced gelation method.

Preparation of Noble Metal Aerogels

The resulting hydrogels were washed and purified with deionized water for 5–6 times and then solvent-exchanged with tert-butanol for 2-3 times. Afterwards, the wet gels were flash-frozen by liquid nitrogen (–196 ºC) and remained for ca. 10 min to enable complete freezing. The frozen samples were put into the chamber of a freeze dryer (TOPTI-12S-80) and dried for 12-24 h at ＜ 1 Pa. The temperature of the cold trap was set to –80 ºC.

Computational Procedures

Au (111) was chosen as the adsorption surface, which exists as the highest peak in XRD. The Au (111) surface composed of three layers of gold atoms was built in a rhombic simulation box of the dimensions x = 17.30 Å, y = 17.30 Å, and z = 54.71 Å. Then, five organic molecules (cetyltrimethylammonium ion: CTA+, citrate ion: CA−, 3-aminopropionic acid: β-Ala, L-cysteine: L-Cys, dopamine: Dop） were placed on the Au (111) surface respectively. Finally, five initially complex systems were constructed in the same cubic simulation lattice as model.

All density functional theory (DFT) calculations in this study were performed using the DMol^3 program package in Materials Studio 8.0. The exchange and correlation terms were determined using the Generalized Gradient Approximation (GGA) in the form proposed by Perdew, Burke, and Ernzerhof (PBE). The DNP version 4.4 basis set was used, while the core electrons of gold were treated by the DFT semi-core preudopots (DSPP) method. A semi-empirical van der Waals correction accounted for the dispersion was included through the use of the DFT-D method of **TS**. Solvation effects were calculated using the COSMO solvation model for all the systems with water as solvent. The global orbital cutoff was set to 4.0 Å, and a 0.005 Ha smearing was used to the orbital occupation. The thresholds of energy, force, and displacement were 10^{-5} Hartree, 2×10^{-3} Hartree/atom for the maximum force, and 5×10^{-3} Å for displacement. Self-consistent field (SCF) procedures were performed with a convergence criterion of 10^{-6} Ha on the total energy to achieve accurate electronic convergence.

The binding energies of organic molecules on Au (111) (E_{binding}) were calculated by the following equation:

$$E_{binding} = E_{ligand-Au(111)} - (E_{ligand} + E_{Au(111)}) \quad (1)$$

where E_{ligand} and $E_{Au\ (111)}$ represent the energies of the single organic molecule and the Au (111) surface, respectively, and $E_{ligand\text{-}Au\ (111)}$ is the total energy of the organic molecule Au (111) complex.

Characterizations

Zeta potential Characterization

Zeta potential tests were performed on a Zetasizer Nano (ZEN5600, Malvern). The original solutions of gold nanoparticles and salts were purified separately with a 0.45-μm filter membrane before the tests. To reflect the real reaction conditions and to avoid possible deviations incurred by dilution, the concentrations of all reactants (metal precursors, ligands, and salts) used here were exactly the same as described in the experimental part.

Microscopy Characterization

To *in situ* observe the nanoparticles forming a hydrogel, the following procedure was applied. The negatively charged metal particles were dropped onto a cover glass to form a droplet. Then, the positively charged metal particles were added to the above droplet. In situ optical imaging was performed on an inverted optical microscope (Carl Zeiss Microscope GmbH) with the magnification of 63×/0.95 M27 objective. For video recording, a corresponding camera from the Carl Zeiss Microscope was employed. Scanning electron microscopy (SEM) and energy- dispersive X-ray spectroscopy (EDX) were performed on a Hitachi FESEM SU8020 scanning electron microscope coupled with a Silicon Drift Detector 80 X-Max^N from Oxford Instruments and operated at 2 kV (for SEM imaging) / 20 kV (for EDX analysis) and 10 μA. Dried gels samples were prepared by directly sticking onto conductive carbon tape or dropcasting them on a Si-Wafer for the EDX measurements. Transmission electron microscopy (TEM) analysis was carried out by using a JEOL JEM 1400 plus microscope operated at 120 kV. Samples were prepared by dispersing in acetone under ultrasonication (15 s to 120 s, depending on their dispersing ability), followed by dropping onto carbon-coated copper-based TEM grids and drying at ambient temperature. High-angle annular dark-field scanning transmission electron microscopy (HAADF-STEM) imaging combined with spectrum imaging analysis based on energy-dispersive X-ray spectroscopy (EDX) were performed at 200 kV with a Talos F200X microscope equipped with an X-FEG electron source and a Super-X EDX detector system (FEI). Prior to (S)TEM analysis, the specimen mounted in a high-visibility low-background holder was placed for 2 s into a Model 1020 Plasma Cleaner (Fischione) to remove possible contaminations.

Diffraction Characterization

X-ray powder diffraction (XRD) was carried out on a Phaser D2 X-ray diffractometer (Bruker) with Cu Kα radiation (λ = 1.5406 Å) in a 2θ range of 20–90°, where symmetrical scans were performed. The samples were dispersed in ethanol and drop-cast on a Si wafer.

Spectroscopy Characterization

Ultraviolet–visible spectroscopy (UV-vis) absorption spectra were recorded on a Cary 60 UV-Vis Spectrophotometer in the UV-vis spectral region (200 ~800 nm)

Element Analysis

Inductively coupled plasma atomic emission spectroscopy (ICP-AES) was performed using an Agilent 720ES optical emission spectrometer.

X-ray photoelectron spectroscopy (XPS) was performed on an Axis Ultra spectrometer (Kratos, UK) with a high-performance Al monochromatic source operated at 15 kV. The XPS spectra were taken after all binding energies were referenced to the C 1s neutral carbon peak at 284.8 eV, and the elemental compositions were determined from the peak area ratios after correction with the sensitivity factors from Casa XPS.

Gas Adsorption Measurements

Nitrogen adsorption experiments were performed with a Quantachrome NOVA 3000e at 77 K. Before the measurements, the samples were outgassed at 323 K for ~24 h under vacuum. A filling rod was used to reduce the dead volume, thus improving the measurement accuracy. The specific surface area was calculated by using the multi-point BET (Brunauer-Emmett-Teller) equation ($0.1 < p/p_0 < 0.3$). The total pore volume was calculated at $p/p_0 = 0.99$, in consistence with the value derived by the BJH (Barret–Joyner–Halender) method. The pore size distribution was derived by using the density functional theory method, which is implanted in the software of the instrument.

Electrochemical Measurements

All electrochemical tests were performed with a three-electrode system on an Autolab/PGSTAT 30 (Eco Chemie B. V. Utrecht, the Netherlands). A glassy carbon electrode (GCE, 3 mm in diameter), Ag/AgCl (saturated KCl aqueous solution) electrode, and platinum foil were used as working electrode, reference electrode, and counter electrode, respectively. For modification of the working electrode, ca. 1 mg catalyst was dispersed in 1 mL of 2-propanol by sonicating for ~30 min to acquire the catalyst ink. Then, a specific amount of ink was transferred on the GCE electrode and evaporated at ambient temperature, followed by coating with 5 μL Nafion (0.5 wt % in ethanol). The concentration of Pd in the ink was determined by ICP-OES, and the final loading of Pd (m_{Pd}) was calculated accordingly to be ~20 μg cm^{-2}. For the commercial Pd/C (20 wt.% Pd on carbon black, Alfa) catalyst, the ink was prepared in the same way, except that the initial concentration in 2-propanol was 4 mg mL^{-1}. Cyclic voltammetry (CV) curves were conducted in nitrogen-saturated 1 M KOH aqueous solution with a voltage window between -1.0 and 0.5 V (vs. AgCl/Ag) and a scanning rate of 100 mV s^{-1}. For electro-oxidation of ethanol, the tests were performed under N_2 atmosphere in 1 M KOH aqueous solution containing 1 M ethanol. CV curves were recorded between -0.9 and 0.3 V (vs. AgCl/Ag) with a scanning rate of 50 mV s^{-1}. The peak current of the forward scanning (from negative to positive potential) and backward scanning are denoted as I_f and I_b, respectively. The stability test was conducted for 10000 s at the potential of the forward peak current maximum.

Catalytic reduction of p-nitrophenol (p-NP)

The catalytic performance of the noble metal aerogels was evaluated using the reduction of p-nitrophenol at room temperature. All aqueous solutions were freshly prepared. A standard catalytic test reaction was carried out in a quartz cell. For the catalytic reduction of p-nitrophenol, 30 µL of p-NP (10 mM) and 150 µL of $NaBH_4$ (2 M) were added to a quartz cell containing 2.97 mL of deionized water. Thereafter, 20 µL of an aqueous solution containing the aerogel catalyst (0.5 mg/mL) was injected into the cell to start the reaction. The intensity of the absorption peak at 400 nm in a Cary 60 UV-Vis spectrophotometer was used to monitor the process of the conversion of p-nitrophenol (p-NP) to p-aminophenol (p-AP). The percentage of the catalytic conversion efficiency (η) of p-NP to p-AP in the reaction process was calculated using the following equation:

$$\eta = \frac{C_0 - C_t}{C_0} * 100$$

where C_t is the concentration of p-NP measured at time t, C_0 is the initial concentration of p-NP measured at time zero.

The catalytic reduction of p-NP follows pseudo-first-order kinetics, the apparent rate constant (K_{app}) can be used as an indicator to assess the catalytic activity of the catalyst, the value was determined by following equation:

$$-\ln\left(\frac{C_t}{C_0}\right) = -\ln\left(\frac{A_t}{A_0}\right) = K_{app}t$$

where A_t and C_t are the absorbance and concentration of p-NP at time t, A_0 and C_0 are the initial absorbance and concentration of p-NP.

Figures

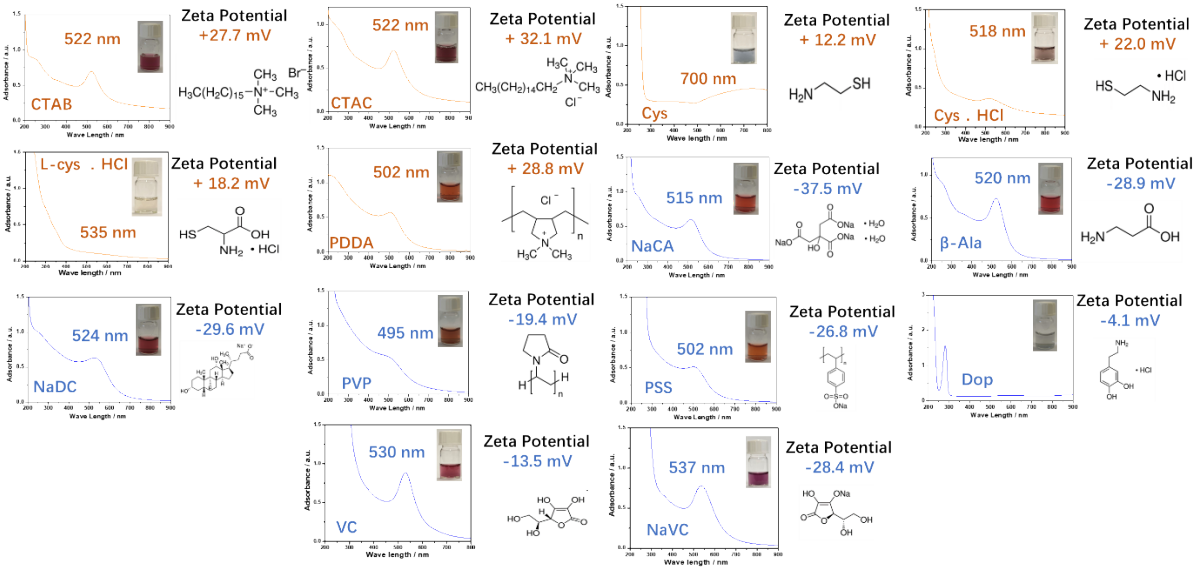

Figure S1. UV-vis absorption spectra, photographs, and zeta potential (ζ) of $HAuCl_4$ aqueous solutions in the presence of various ligands upon addition of $NaBH_4$ reductant. (The ratio of metal salt (M), C_M = 0.2 mM, ligand (L), and reductant (R) was fixed at 1/10/4, the ligand/gold ratio was fixed at 10/1, CTAB/gold = 0.5/1, Dop/gold = 2.5/1, the molecular structures of the ligands are provided.)

	CTAB 0.02 M	CTAC 0.75M	Cys 0.4 M	Cys . HCl 0.4 M	L-cys . HCl 0.4M	PDDA 0.4M
NaCA	+1.5	+1.9	-3.5	-11.3	-27.2	+1.7
β-Ala	+24.5	+30.8	+11.2	+27.2	+4.6	+25.8
NaDC	-11.9	+23.0	-4.5	-17.4	-16.2	+22.3
PVP	+0.4	+33.8	-1.8	+9.0	+10.4	+23.9
PSS	-33.3	+23.3	-16.1	-23.0	-36.2	+17.1
Dop	+13.3	+5.8	+3.9	+15.6	+11.7	+27.1
VC	+25.3	+22.3	+2.6	+16.5	+12.8	+26.3
NaVC	+14.0	+32.6	-15.6	+6.6	+4.2	+25.8

Yellow: Au NPs with different ligands form a gel after 1 day. Blue: Au NPs with different ligands form metastable colloids with precipitation after 1 day. Grey: Au NPs with different ligands form stable colloids without precipitation. Zeta potential of mixed ligand-stabilized Au NPs after mixing procedure for *ca.* 5 min.

Figure S2. Zeta potential (ζ) values (in mV) of gold NP solutions (C_M = 0.2 mM) after mixing procedure.

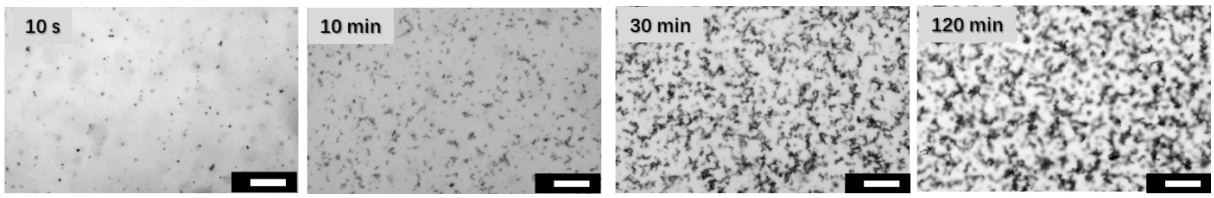

Figure S3. In situ optical microscopy characterization during gelation of Au NP solutions (C_M = 0.2 mM) after mixing two different ligands (NaCA, and CTAB). The scale bars are 20 μm.

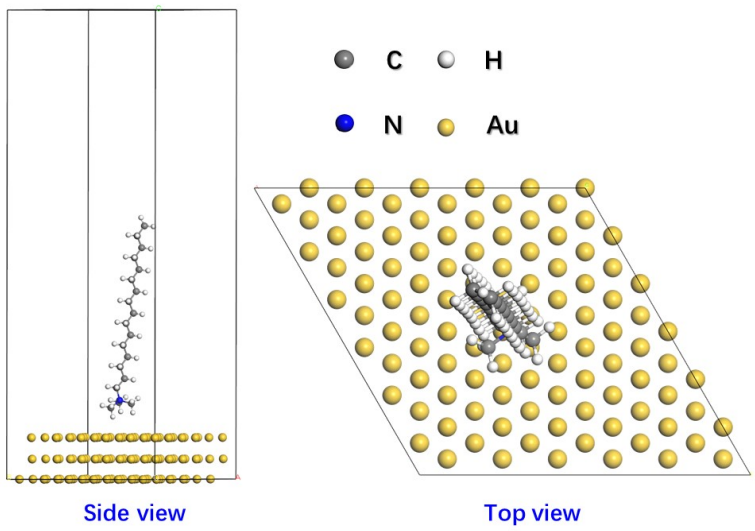

Figure S4. Optimized structure of CTA+ adsorbed on an Au (111) surface.

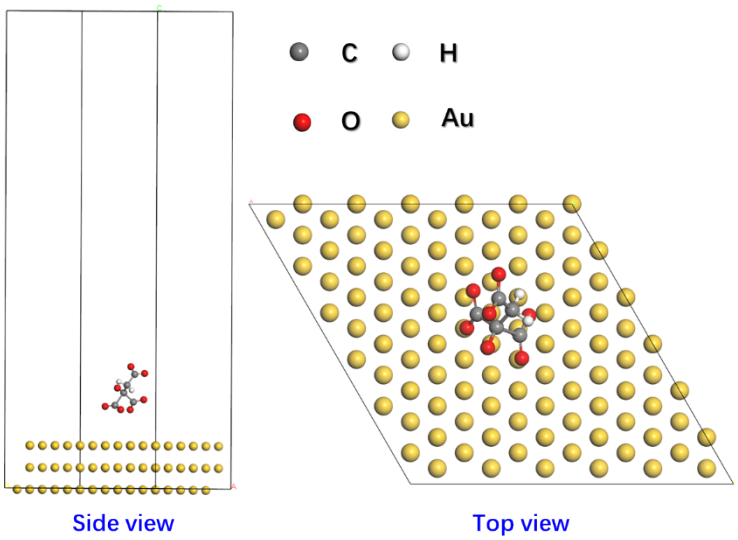

Figure S5. Optimized structure of citrate (CA-) adsorbed on an Au (111) surface.

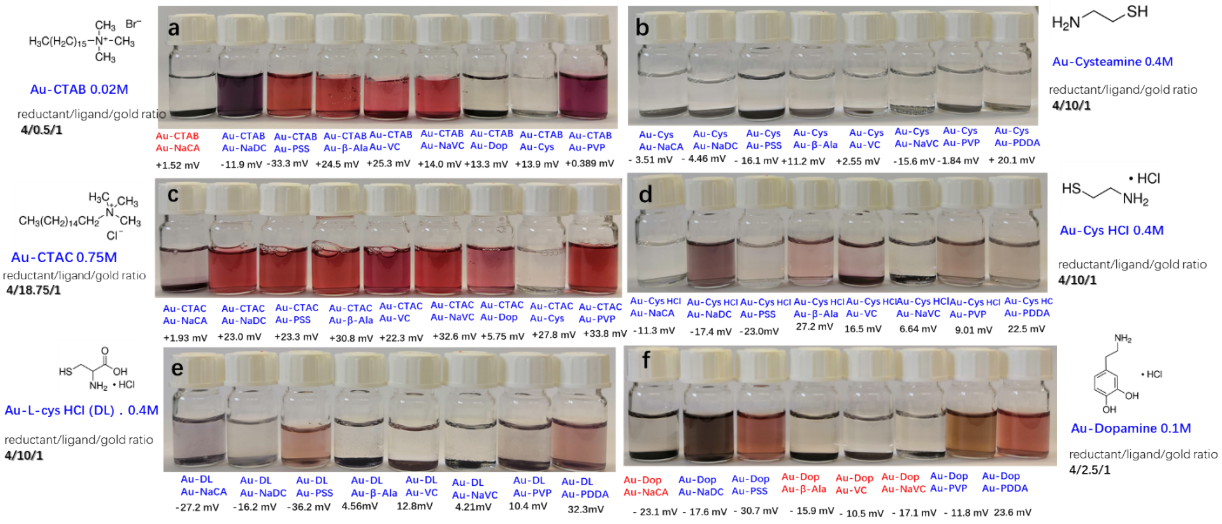

Figure S6. Destabilization of gold NP solutions (C_M = 0.2 mM) with oppositely charged particles (zeta potential values (in mV) of mixed ligand-stabilized gold NPs after 5 min of mixing, photos of gold NPs were taken after grounding for 1 day). (a) CTAB, (b) Cys, (c) CTAC, (d) Cys.HCl, (e) L-Cys.HCl, and (f) Dop.

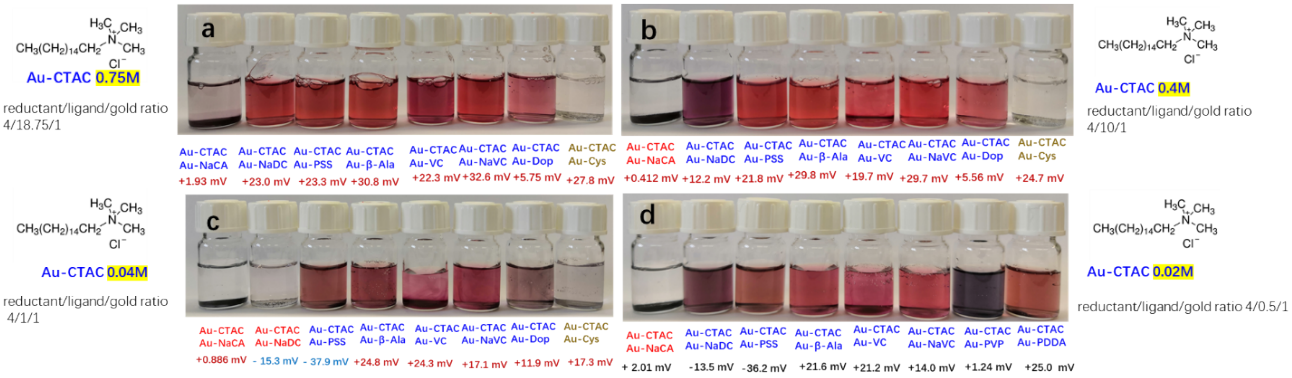

Figure S7. Destabilization of CTAC-stabilized gold NP solutions with different ligand concentrations (ligand/metal) (C_M = 0.2 mM, ligand concentrations (a) L/M = 18.75, (b) L/M = 10, (c) L/M = 4, and (d) L/M = 0.5) with oppositely charged particles (the ligand/gold ratio was fixed at 10/1, zeta potential values (in mV) of mixed ligand-stabilized gold NPs after 5 min of mixing, photos of gold NPs were taken after grounding for 1 day).

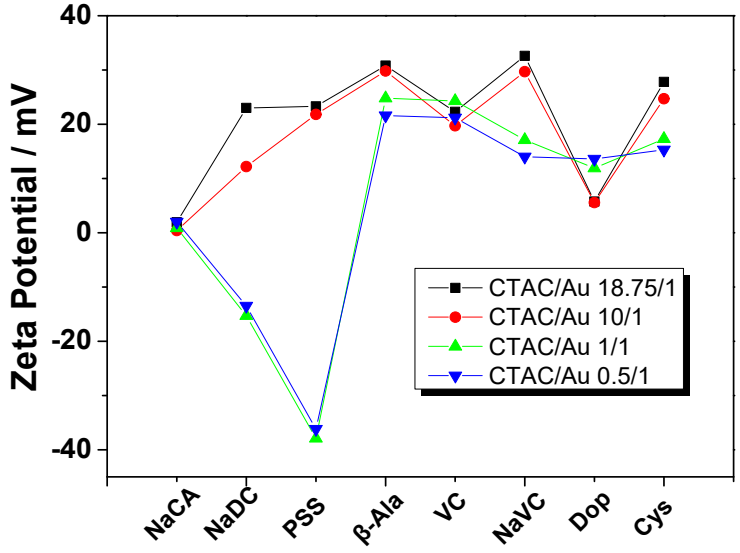

Figure S8. Zeta potential of various mixed ligand-stabilized gold NP solutions after 5 min of mixing (Variation of the ligand/gold ratio for the p-Au NPs in a range of 18.75 to 0.5, while the ligand ratio for the n-Au NPs is fixed at 10/1., these zeta potentials correspond to the experiment from figure S7).

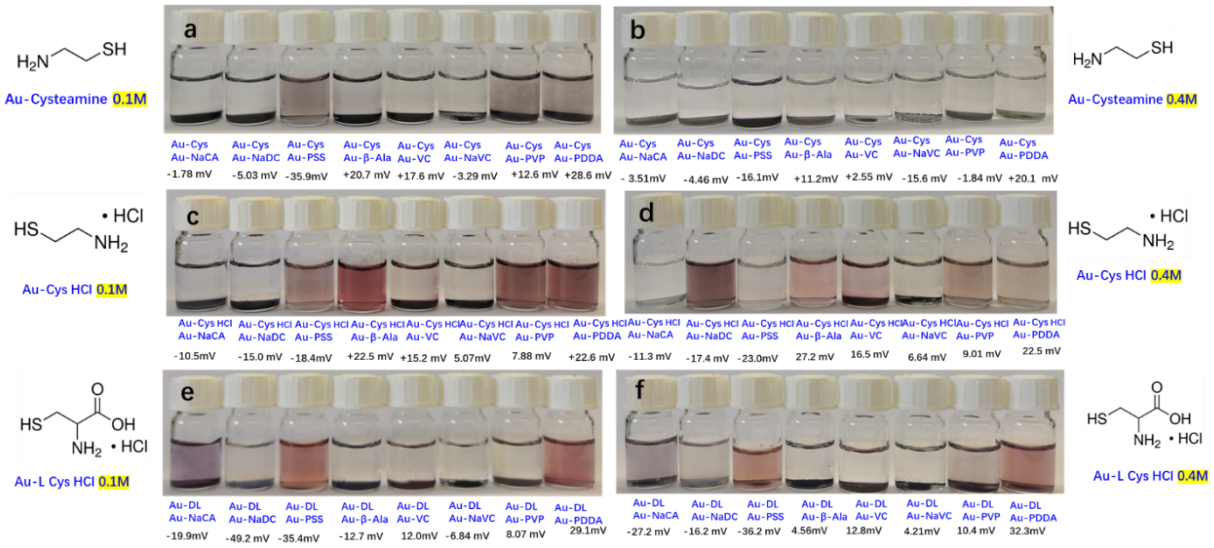

Figure S9. Destabilization of various ligand-stabilized gold NP solutions (C_M = 0.2 mM, ligand concentrations 0.1 M: ligand/gold ratio was fixed at 2.5/1, 0.4 M: ligand/gold ratio was fixed at 10/1) with oppositely charged particles (zeta potential values (in mV) of mixed ligand-stabilized gold NPs after 5 min of mixing, photos of gold NPs were taken after grounding for 1 day).

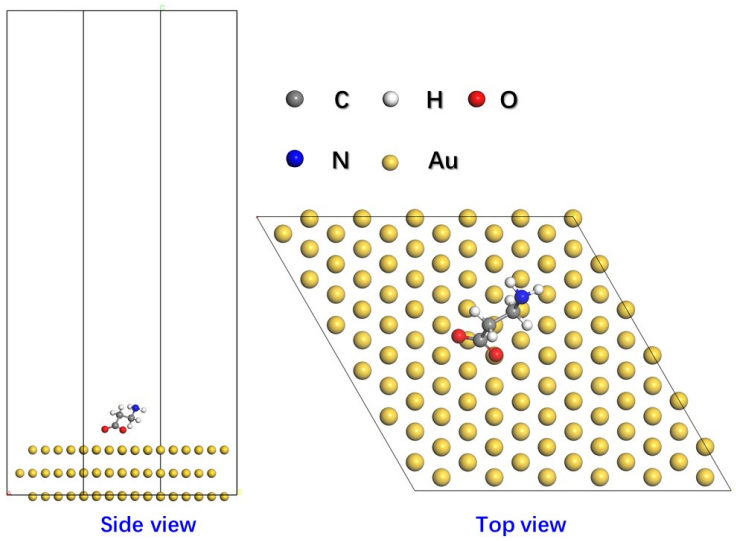

Figure S10. Optimized structure of β-Ala adsorbed on an Au (111) surface.

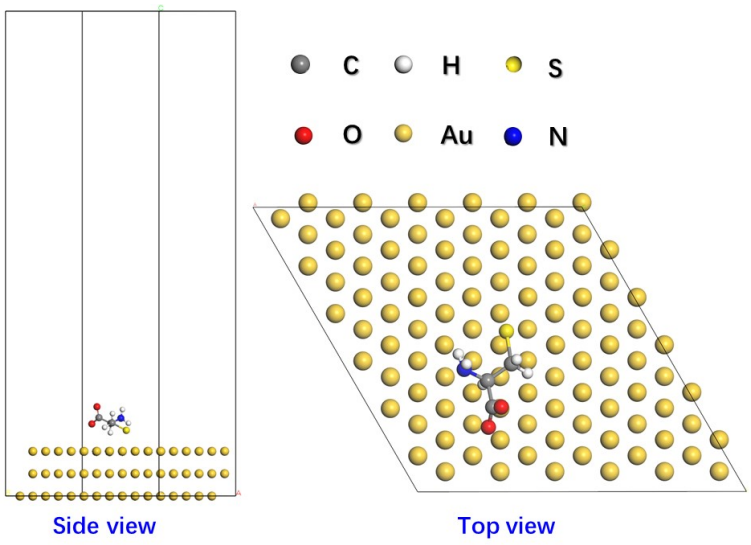

Figure S11. Optimized structure of L-cysteine adsorbed on an Au (111) surface.

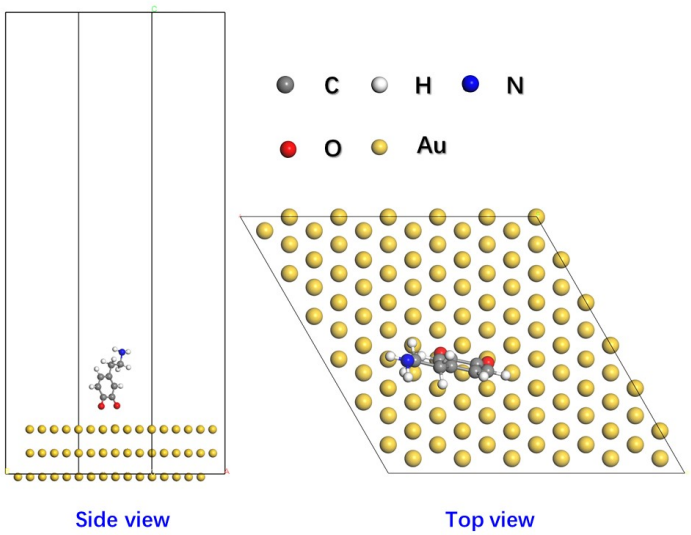

Figure S12. Optimized structure of Dop adsorbed on an Au (111) surface.

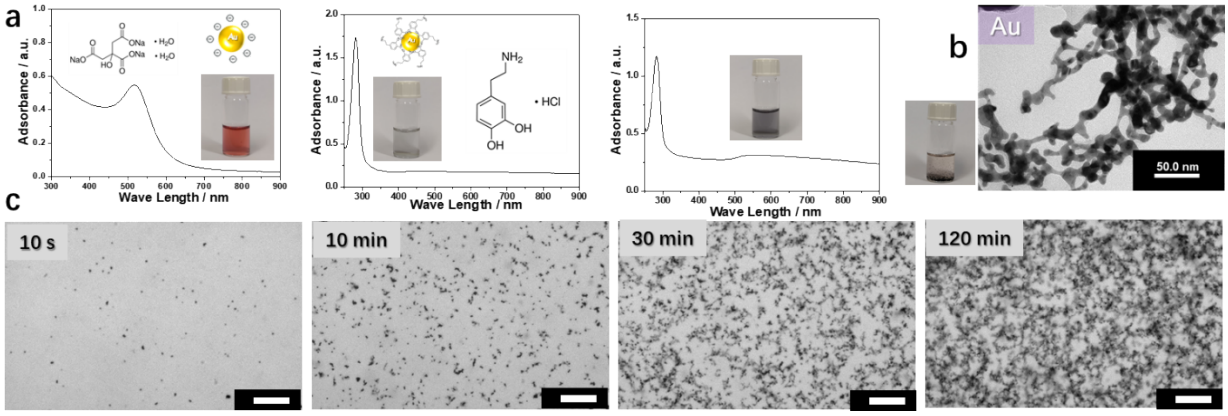

Figure S13. Fabrication process of a gold gel by dopamine-induced gelation. (a) UV-vis absorption spectra of the Au nanoparticle solutions (C_M = 0.2 mM) with two different ligands (trisodium citrate and dopamine hydrochloride) before and after mixing (inset: photos of solutions and chemical structures of the ligands). (b) TEM image and photo of the gold aerogel by leaving the solution for more than five hours. (c) In situ optical microscopy characterization during gelation of the Au nanoparticles.

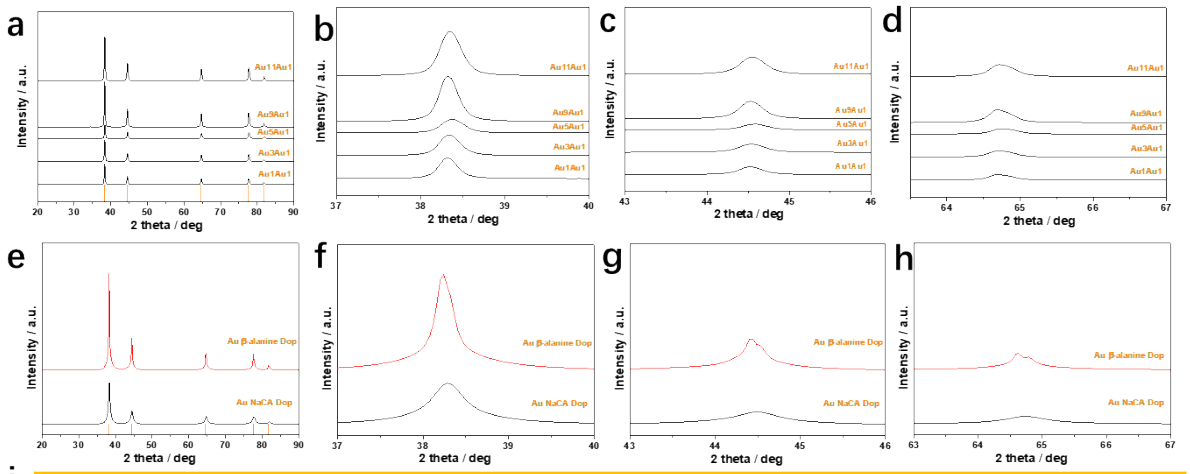

i

Entry	Au1Au1	Au3Au1	Au5Au1	Au9Au1	Au11Au1	Au NaCA Dop	Au β-ala Dop
Crystallite size	20.3 nm	28.1 nm	29.8 nm	30.8 nm	31.8 nm	6.5 nm	7.7 nm

Figure S14. XRD patterns of gold aerogels obtained by electrostatic interaction (a-d) and dopamine-induced gelation (e-h). XRD patterns of all gold aerogels (a and e) exhibit five peaks which can be indexed as the (111, (b and f)), (200, (c and g)), (220, (d and h)), (311), and (222) reflections of the face-centered cubic structure of crystalline Au. The Au reference pattern is PDF#04-0784. For the XRD tests a-h, the full width at half maximum (FWHM) reflects the crystallite size (i) of the corresponding materials with different ratios.

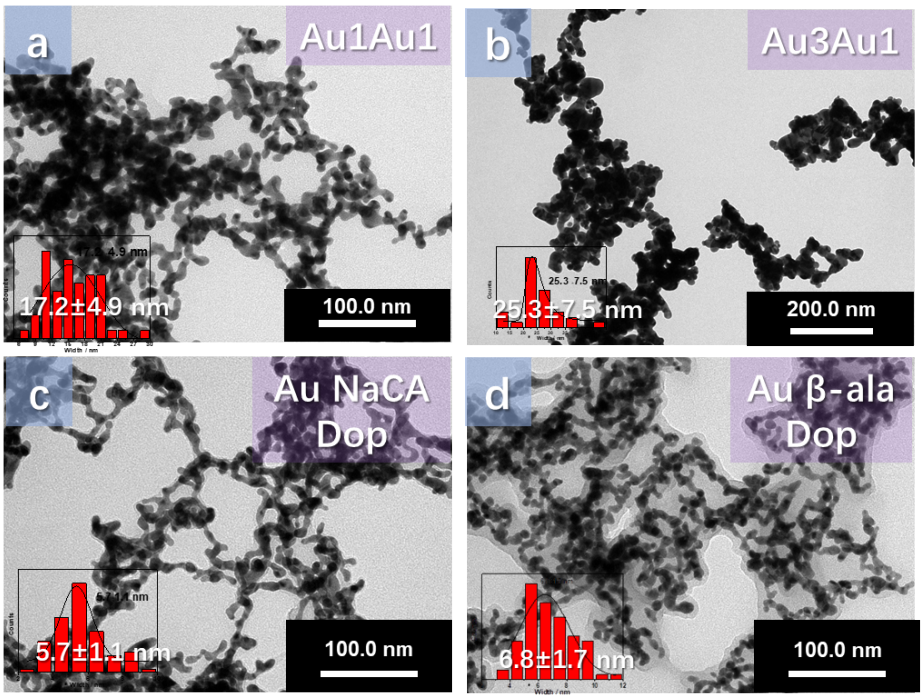

Figure S15. TEM images and ligament size distributions (insets) of gold aerogels of CTAB/NaCA by electrostatic interaction (a, b) and dopamine-induced gelation (c, d).

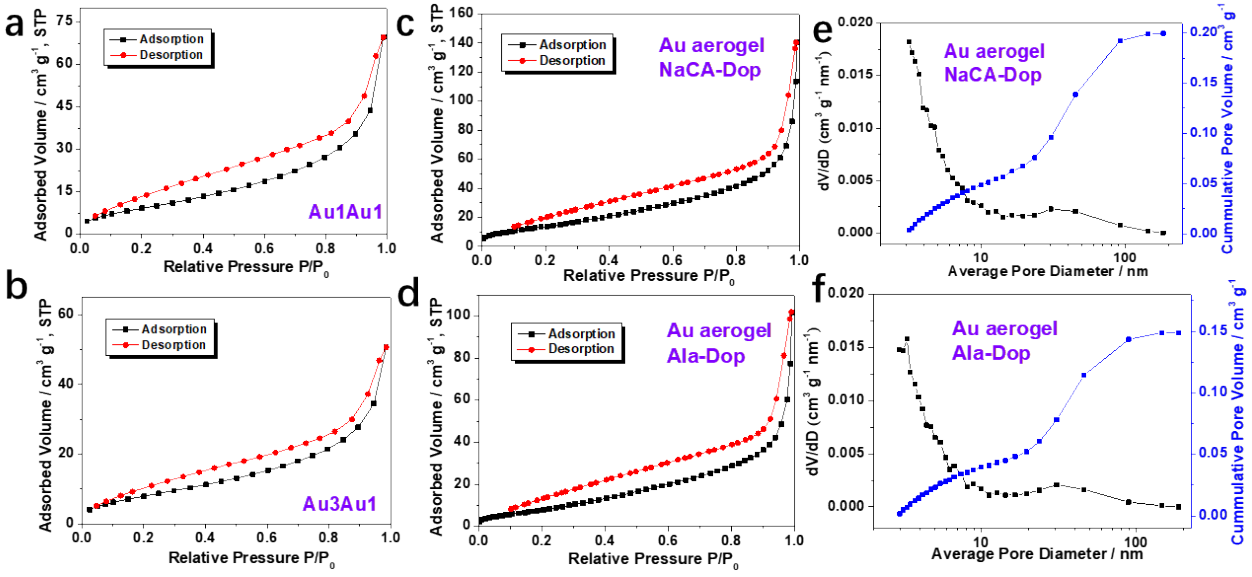

Figure S16. Nitrogen adsorption curves and pore size distributions (PSD) of various gold aerogels obtained by electrostatic interaction (a + b without, c + d with dopamine) and their corresponding pore size distributions (e + f).

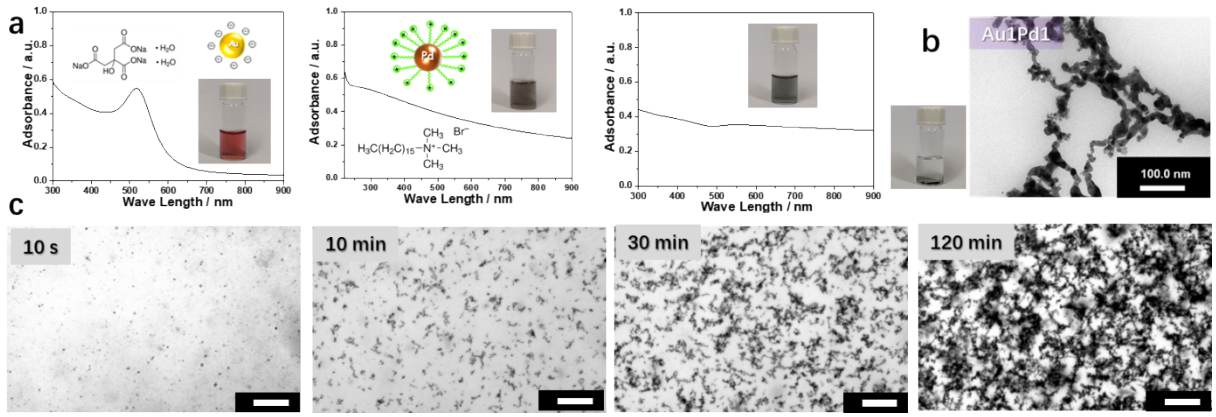

Figure S17. Fabrication process of Au-Pd gels by electrostatic interaction. (a) UV-vis absorption spectra of the Au and Pd NPs (C_M = 0.2 mM) solutions before and after mixing (inset: photos of solutions and chemical structures of the ligands: trisodium citrate for Au nanoparticles and cetyltrimethylammonium bromide for Pd nanoparticles). (b) TEM image and digital photo of the Au1Pd1 aerogel. (c) In situ optical microscopy characterization during gelation of the nanoparticles.

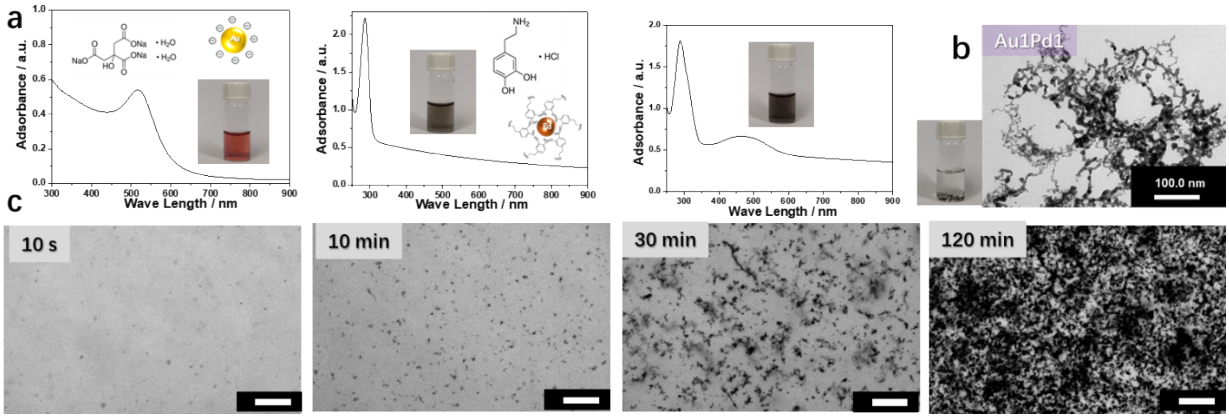

Figure S18. Fabrication process of Au-Pd gels by dopamine-induced gelation. (a) UV-vis absorption spectra of the Au and Pd NPs (C_M = 0.2 mM) solutions before and after mixing (inset: photos of solutions and chemical structures). (b) TEM image and digital photo of the Au-Pd aerogel with two different ligands (trisodium citrate for Au nanoparticles and dopamine hydrochloride for Pd nanoparticles). (c) In situ optical microscopy characterization during gelation of the nanoparticles.

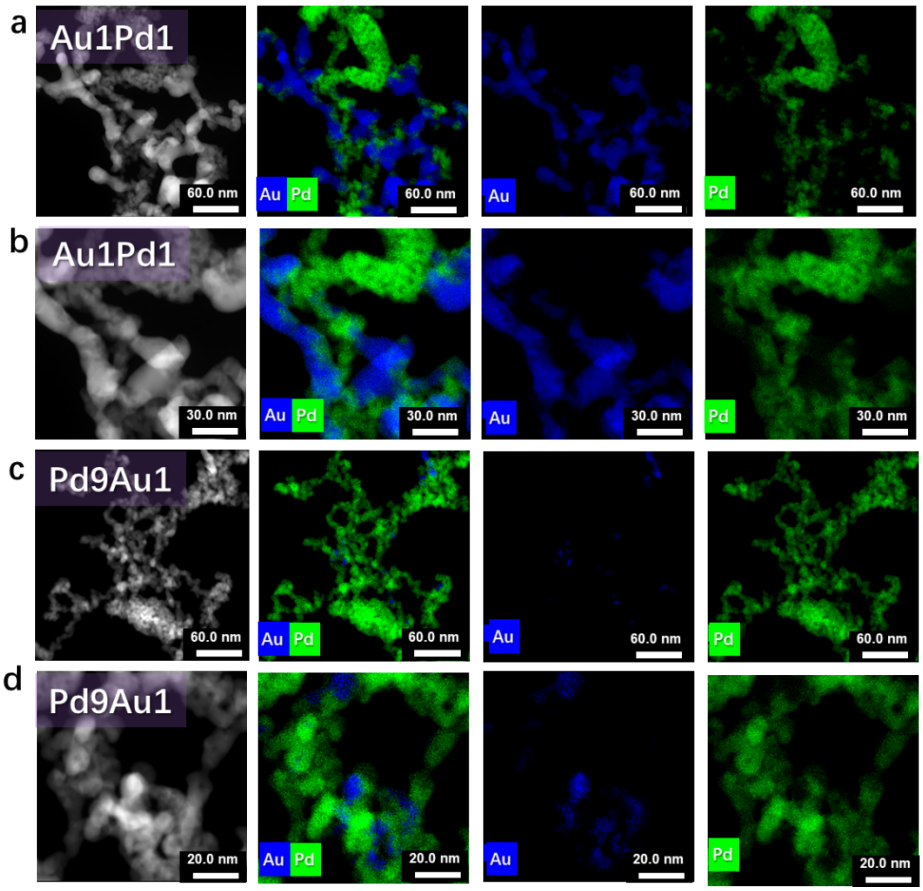

Figure S19. HAADF-STEM images and the corresponding EDX-based element distributions of the indicated Au-Pd aerogels prepared by the electrostatic interaction gelation method.

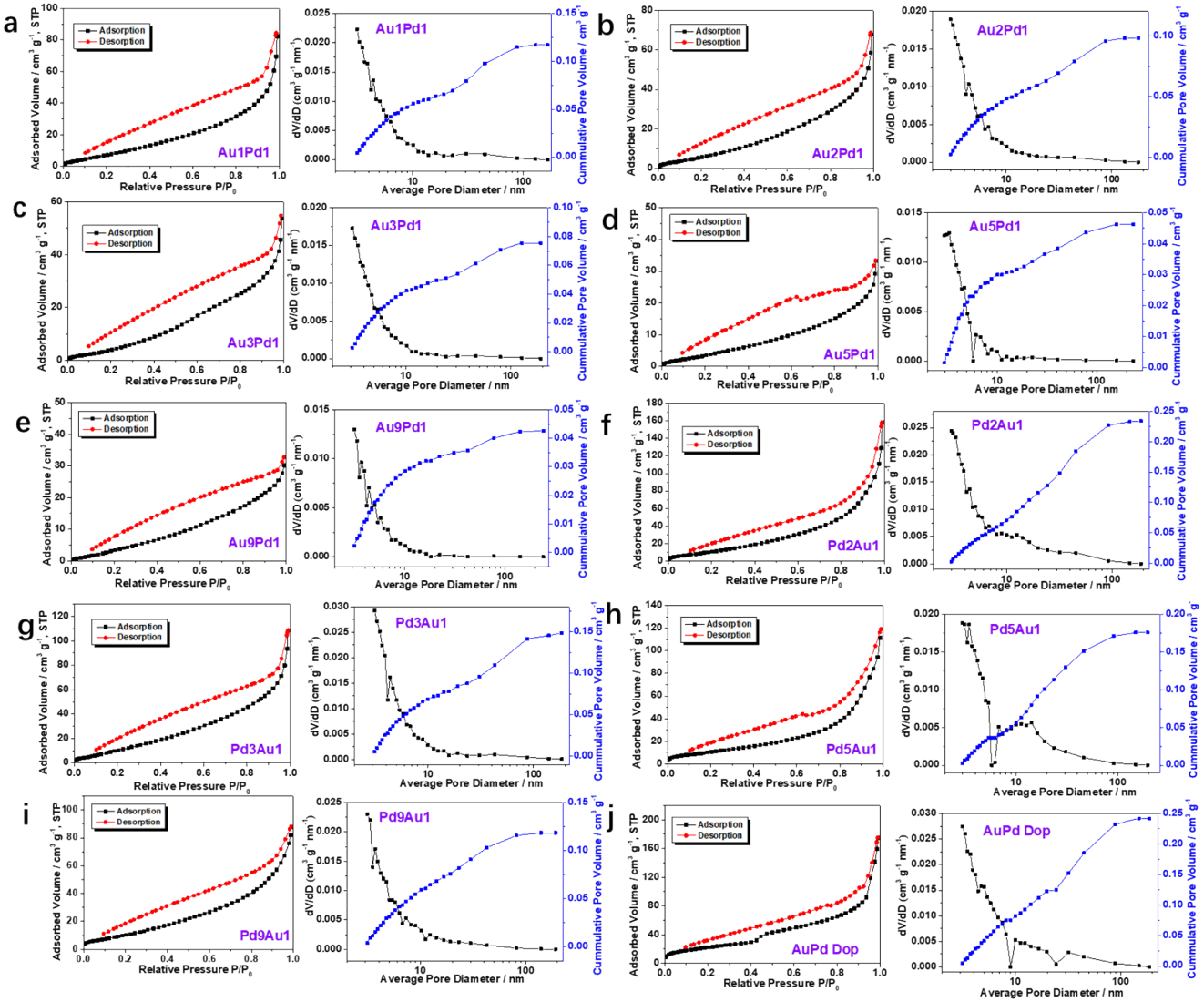

Figure S20. Nitrogen adsorption isotherms and the corresponding pore size distributions obtained by the BJH method for the Au-Pd aerogels.

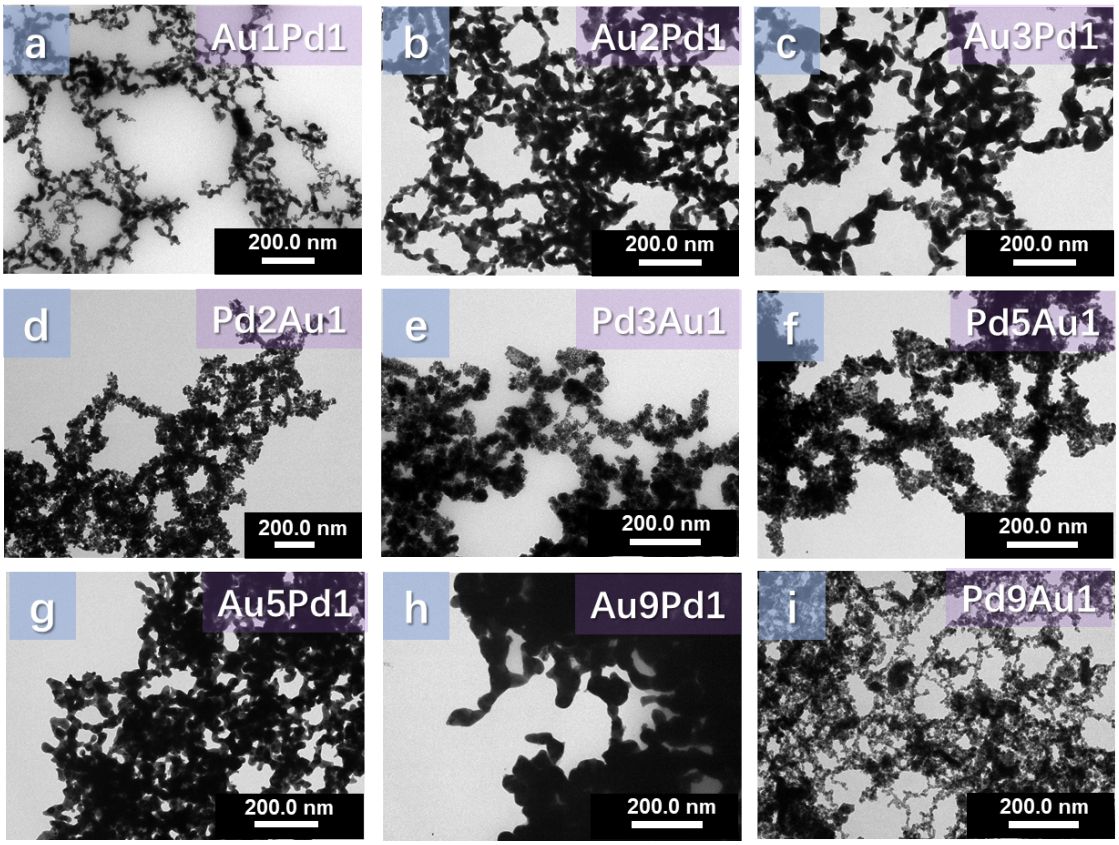

Figure S21. TEM images of the indicated Au-Pd aerogels with different Au/Pd ratios (without dopamine).

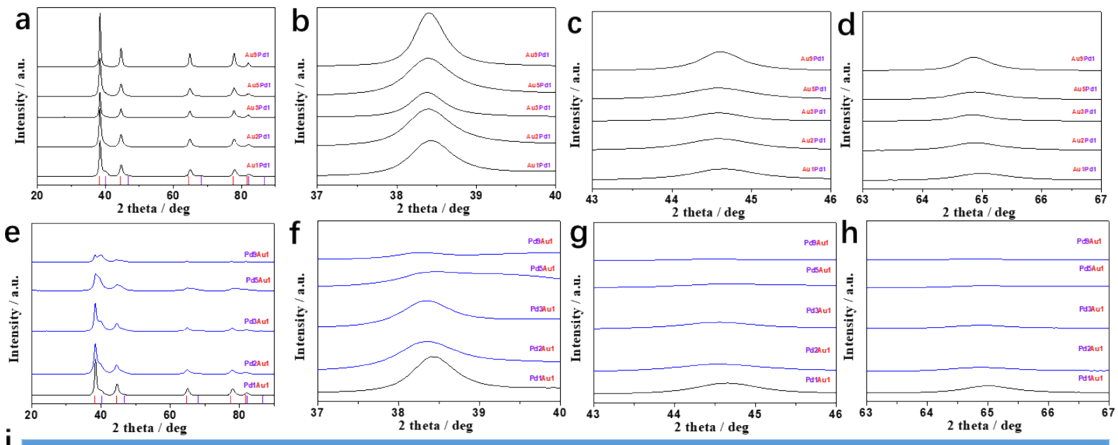

i

Entry	Au1Pd1	Au2Pd1	Au3Pd1	Au5Pd1	Au9Pd1	Pd2Au1	Pd3Au1	Pd5Au1	Pd9Au1
Crystallite size	8.5 nm	9.9 nm	12.9 nm	13.8 nm	17.2 nm	6.2 nm	6.0 nm	3.5 nm	2.3 nm

Figure S22. XRD patterns of Au-Pd aerogels obtained by electrostatic interaction. XRD patterns of all Au-Pd aerogels (a and e) with special focus to the 111 reflection (b and f), 200 reflection (c and g), and 220 reflection (d and h). The indicated reference patterns are PDF#04-0784 (Au) and PDF#46-1043 (Pd). For the XRD tests a-h) the full width at half maximum (FWHM) reflects the crystallite size (i) of the corresponding materials with different Au/Pd ratios.

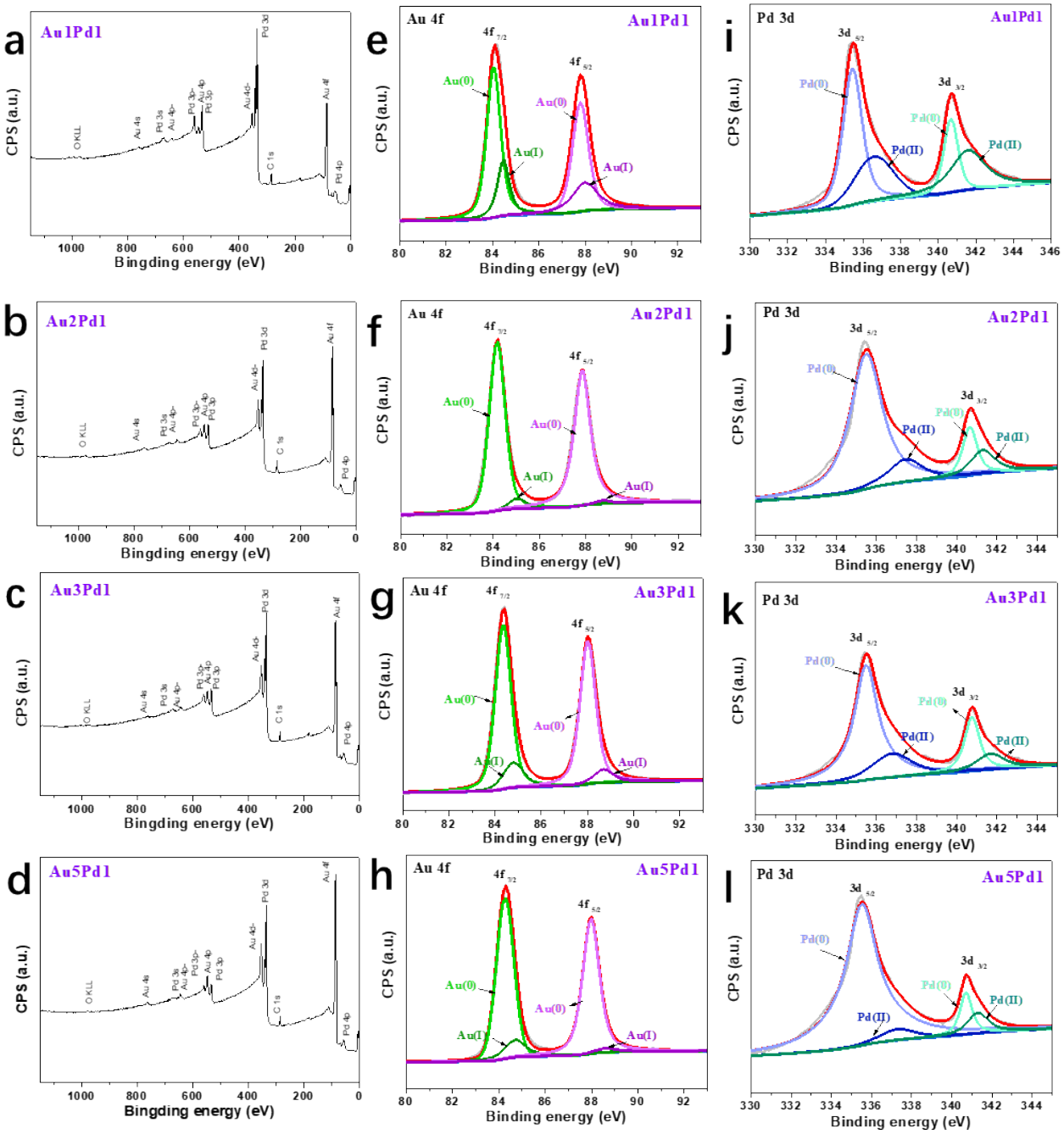

Figure S23. (a-d) Full XPS spectra, (e-h) high-resolution gold spectra, and (i-l) high-resolution palladium spectra of the indicated aerogels without dopamine.

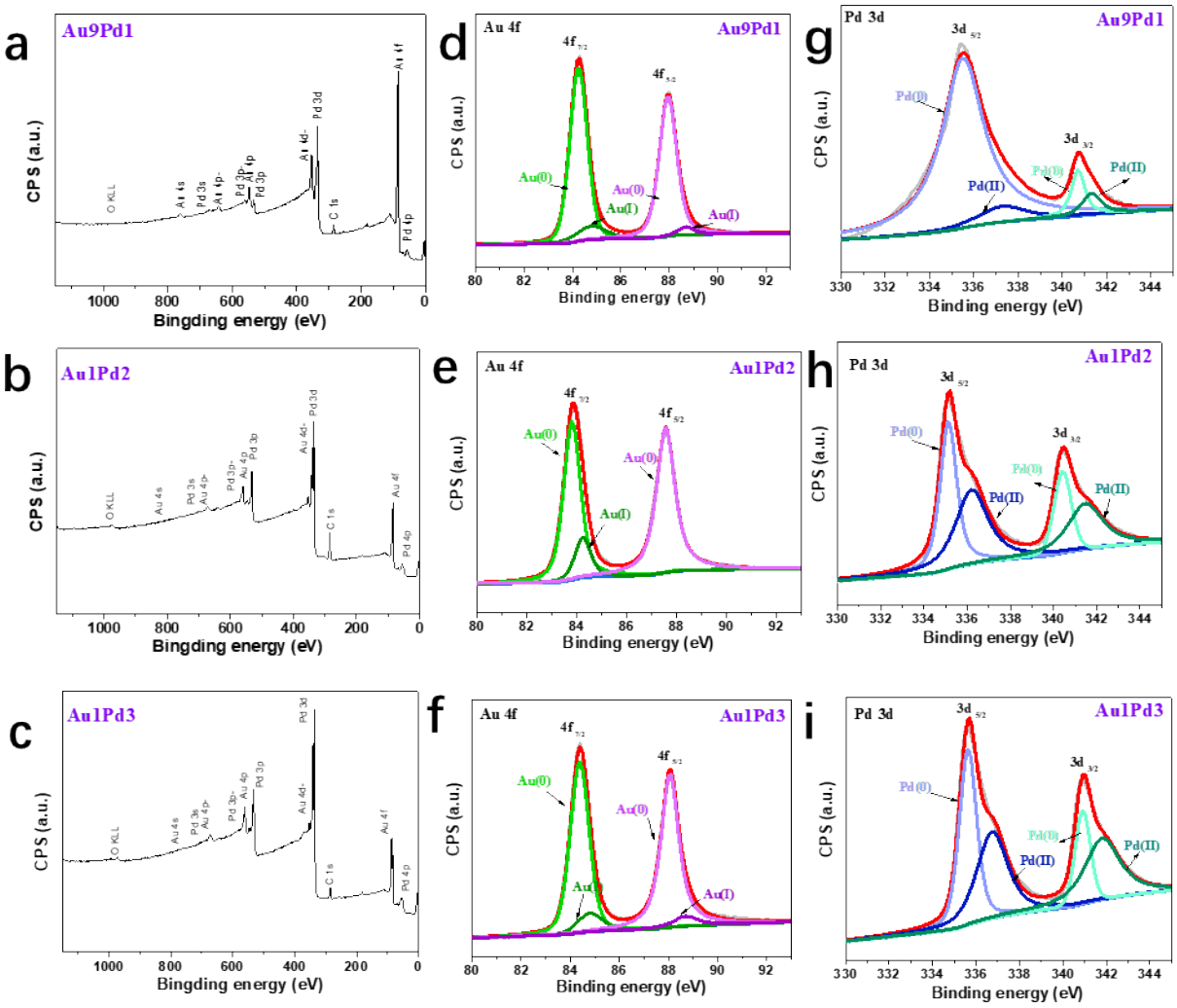

Figure S24. (a-c) Full XPS spectra, (d-f) high-resolution gold spectra, and (g-i) high-resolution palladium spectra of the indicated aerogels without dopamine.

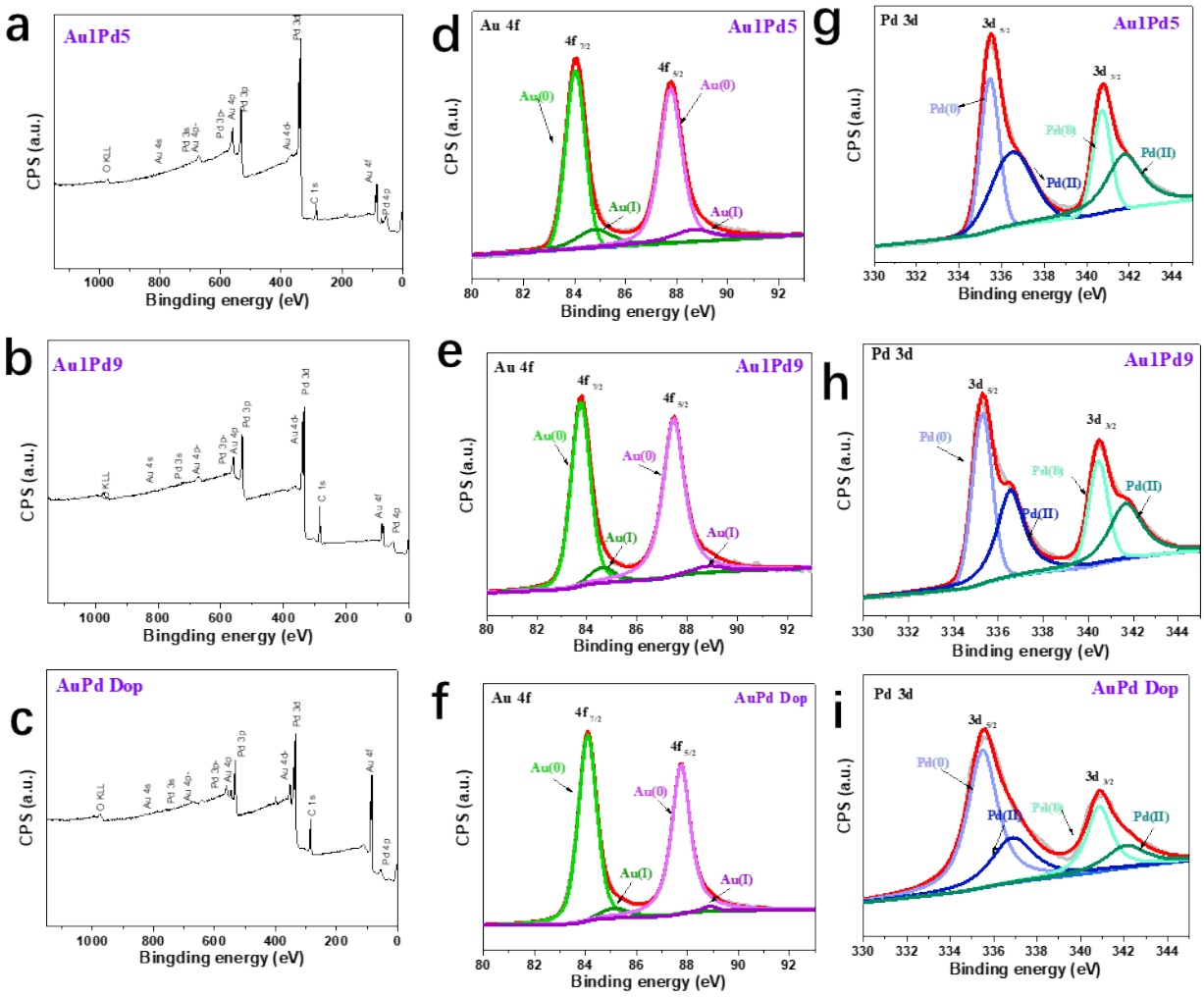

Figure S25. (a-c) Full XPS spectra, (d-f) high-resolution gold spectra, and (g-i) high-resolution palladium spectra of the indicated aerogels (a-b, d-e, g-h without, c + f + i with dopamine).

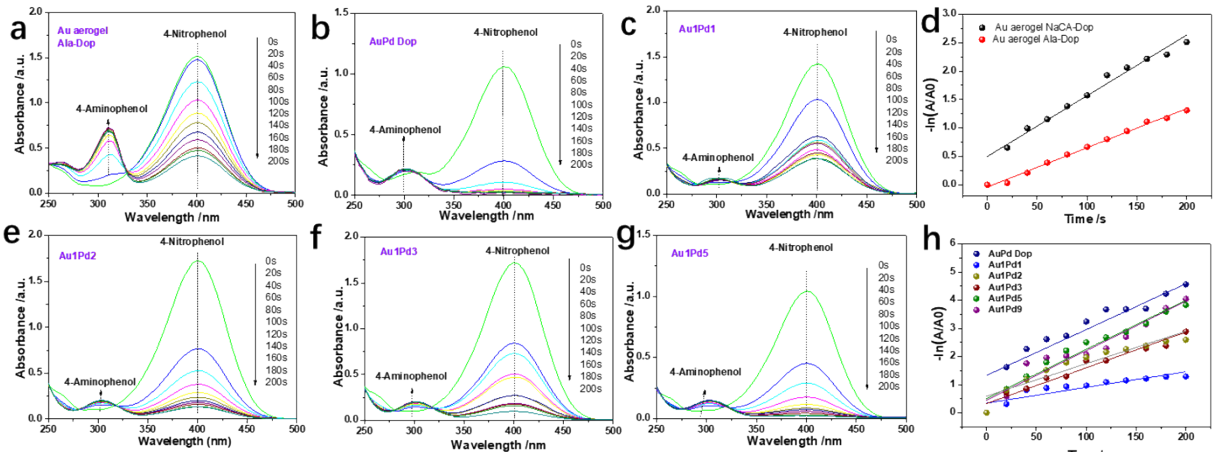

Figure S26. (a-c) and (e-g) UV-vis spectra of the reduction of p-nitrophenol in aqueous solution recorded every 1 min using different samples. (d) and (h) Plot of $-\ln(A_t/A_0)$ versus

the reduction time t using different samples (Au1PdX, X=1,2,3,5,9, without dopamine; AuPd Dop, with dopamine).

Tables

Table S1. Zeta potential (ζ) values (in mV) of gold NP solutions (C_M = 0.2 mM) before mixing.

Cationic Ligand	**CTAB**	**CTAC**	**Cys**	**Cys. HCl**	**L-cys. HCl**	**PDDA**
Chemical Name	Cetyltrimethylammonium bromide	Cetyltrimethylammonium chloride	Cysteamine	Cysteamine Hydrochloride	L-Cysteine hydrochloride	Poly(diallyldimethylammonium chloride)
Zeta Potential (mV)	**+27.7**	**+32.1**	**+12.2**	**+22.00**	**+18.2**	**+28.8**

Anionic Ligand	**NaCA**	**β-Ala**	**NaDC**	**PVP**	**PSS**	**Dop**	**VC**	**NaVC**
Chemical Name	Sodium citrate	3-Aminopropionic acid	Sodium deoxycholate	Polyvinylpyrrolidone	Poly(sodium 4-styrenesulfonate)	Dopamine hydrochloride	L-Ascorbic acid	Sodium ascorbate
Zeta Potential (mV)	**-37.5**	**-28.9**	**-29.6**	**-19.4**	**-26.8**	**-4.1**	**-13.5**	**-28.4**

Table S2. Binding energies of five organic molecules on Au (111) ($E_{binding}$).

System	E_{ligand} **(a.u)**	$E_{Au\ (111)}$ **(a.u)**	$E_{ligand\text{-}Au\ (111)}$ **(a.u)**	$E_{binding}$ **(a.u)**	$E_{binding}$ **(eV)**
Au (111) -CTA+	-802.22	-22866.15	-23668.39	-0.024	**-0.67**
Au (111) -CA−	-717.79	-22866.15	-23583.96	-0.013	**-0.36**
Au (111) -β-Ala	-322.46	-22866.15	-23188.63	-0.016	**-0.43**
Au (111) -L-Cys	-720.13	-22866.15	-23586.30	-0.023	**-0.65**
Au (111) -Dop	-514.79	-22866.15	-23380.96	-0.014	**-0.39**

Table S3. Summary of nitrogen adsorption data and ligament sizes of as-prepared gold aerogels.

Entry	Metals	A-Ligands	B-Ligands	A/B Ratio	S_{BET} (m^2g^{-1})	S_{BET} (m^2mol^{-1})	V_{tot} ($cm^3\ g^{-1}$)	d (nm)
1	Au	NaCA	CTAB	1:1	25.3	4988.04	0.047	17.2±4.9
2	Au	NaCA	CTAB	3:1	11.1	2188.67	0.032	25.3±7.5
3	Au	NaCA	CTAB	5:1	7.2	1414.46	0.022	25.4±7.9
4	Au	NaCA	CTAB	9:1	5.52	1087.44	0.023	26.1±8.2
5	Au	NaCA	CTAB	11:1	5.48	1079.56	0.020	27.2±9.3
6	Au	NaCA	Dopamine	1:1	57.4	11311.74	0.217	5.7±1.1
7	Au	β-alanine	Dopamine	1:1	37.7	7432.81	0.158	6.8±1.7

Note: The specific surface area (S_{BET}) was obtained from N_2-physisorption measurements. The average ligament size d was obtained from a statistic analysis of TEM images.

Table S4. Summary of nitrogen adsorption data and ligament sizes of as-prepared Au-Pd aerogels by electrostatic interaction.

Entry	Metal-Ligands	Metal-Ligands	Au/Pd Ratio	S_{BET} (m^2g^{-1})	S_{BET} (m^2mol^{-1})	V_{tot} ($cm^3\ g^{-1}$)	d_{Au} (nm)	d_{Pd} (nm)
1	Au-NaCA	Pd-CTAB	1:1	41.6	6310.1	0.13	15.8±4.6	5.6±1.4
2	Au-NaCA	Pd-CTAB	2:1	34.2	5702.7	0.11	19.6±4.8	6.9±1.9
3	Au-NaCA	Pd-CTAB	3:1	31.7	5519.2	0.08	25.9±6.4	6.4±2.2
4	Au-NaCA	Pd-CTAB	5:1	28.0	5259.1	0.05	19.8±5.5	
5	Au-NaCA	Pd-CTAB	9:1	22.5	4091.7	0.07	37.1±10.5	
6	Au-NaCA	Pd-CTAB	1:2	56.1	7656.8	0.24	14.8±5.5	8.4±2.5
7	Au-NaCA	Pd-CTAB	1:3	63.2	8152.2	0.17	21.9±4.3	6.3±1.7
8	Au-NaCA	Pd-CTAB	1:5	67.3	8171.3	0.25	7.3±1.9	
9	Au-NaCA	Pd-CTAB	1:9	97.3	11235.1	0.14	7.1±1.9	
10	Au-NaCA	Pd-Dopamine	1:1	82.4	12504.6	0.27	6.3 ± 1.8	4.0 ± 1.2

Note: The specific surface area (S_{BET}) was obtained from N_2-physisorption measurements. The average ligament size d was obtained from a statistic analysis of TEM images.

Table S5. Molar ratio of Au, Pd in the bimetallic aerogels Au-Pd obtained using ICP-AES and SEM-EDX.

Aerogel Name	Au/Pd molar ratio	ICP-AES Au/Pd (%)	SEM-EDX* Au/Pd (%)
Au1Pd1	1/1	1.04/1	1.09/1
Au2Pd1	2/1	2.13/1	1.83/1
Au3Pd1	3/1	3.19/1	2.69/1
Au5Pd1	5/1	5.42/1	4.96/1
Au9Pd1	9/1	9.31/1	8.71/1
Pd2Au1	1/2	1/1.95	1/2.18
Pd3Au1	1/3	1/2.85	1/3.09
Pd5Au1	1/5	1/4.88	1/5.22
Pd9Au1	1/9	1/9.59	1/9.20

* The value was estimated by averaging the values from at least 12 areas in one aerogel sample.

Table S6. Comparison of various gold aerogels reported in the literature.

Materials	Methods	Gelation Time	Size (nm)	Surface area (m^2g^{-1})	Factor of adjustable structure	Ref
Au aerogels	Electrostatic Manipulation	1-12h	5.7-27.2	5.5-57.4	Different volume ratios of precursor	This work
Au aerogels	H_2O_2	~1 week	100-500	Very small	/	12
Au aerogels	Excessive $NaBH_4$	2~12 h	4.8-38.3	3.5-59.8	Different ligands	13
Au aerogels	Dopamine	6~72 h	5-6	50.1	/	14
Au aerogels	Salts	4-48 h	6.9-113.7	2.5-29.7	Different salts as initiator	15
Au aerogels	$NaBH_4$, NaH_2PO_2, or dimethylamine borane	A few minutes	63.7±36.0	3.1	/	16
Au aerogels	Hydrazine, 333 K	Several hours	21±11	/	/	17
Au aerogels	Microwave-assisted	Several seconds	2−50	6.5	/	18
Au aerogels	Freeze-thaw	12-24 h	16.8-35	/	/	19
Au aerogels	Salts or $NaBH_4$ under a disturbing environment	4min	18.1±3.0	5.6	/	20
Au aerogels	Ultrasonic-Method& $NaBH_4$	12-50s	3.1-34.4	4.65	/	21

Table S7. Comparison of aerogel performance towards ethanol oxidation in alkaline environment.

Materials	Methods	ratios	I_f (A/mg)	Ref
Au-Pd	Electrostatic Manipulation	1:1	6.6	This work
Au-Pd	Excessive $NaBH_4$	1:1	8.45	13
Au-Pd Au-Pd-Pt	Salts	1:1 1:1:1	2.65 4.82	15
Au-Pd-Pt	Microwave-assisted	1:1:1	8.8	18
Au-Pt Au-Pd	Freeze-thaw	1:1 1:1	3.5 8.4	19
Au-Pd-Pt	Salts or $NaBH_4$ under a disturbing environment	1:1:1	9.1	9
Au-Pd-Pt Au-Pd	Ultrasonic- Method& $NaBH_4$	1:1:1 1:1	4.97 2.45	10

Movies

Movie S1. Gelation motion of gold NP solutions after mixing two different ligands (NaCA, and CTAB). (.AVI format)

Movie S2. Gelation motion of NaCA-stabilized gold NPs mixed with a gold NP solution in the presence of dopamine. (.AVI format)

Movie S3. Gelation motion of NaCA-stabilized gold NPs and CTAB-stabilized palladium NPs. (.AVI format)

Movie S4. Gelation motion of NaCA-stabilized gold NPs and dopamine-stabilized palladium NPs. (.AVI format)

References

[1] J. P. Perdew, K. Burke and M. Ernzerhof, *Phys. Rev. Lett.,* 1996, **77**, 3865.

[2] B. Delley, *Phys. Rev. B.,* 2002, **66**, 155125.

[3] A. Tkatchenko and M. Scheffler, *Phys. Rev. Lett.*, 2009, **102**, 073005.

[4] M. R. Narouz, K. M. Osten, P. J. Unsworth, R. W. Y. Man, K. Salorinne, S. Takano, R. Tomihara, S. Kaappa, S. Malola, C.-T. Dinh, J. D. Padmos, K. Ayoo, P. J. Garrett, M. Nambo, J. H. Horton, E. H. Sargent, H. Häkkinen, T. Tsukuda and C. M. Crudden, *Nat. Chem.,* 2019, **11**, 419-425.

[5] X. Zhu, Q. Guo, Y. Sun, S. Chen, J. Wang, M. Wu, W. Fu, Y. Tang, X. Duan, D. Chen and Y. Wan, *Nat Commun.,* 2019, **10**, 1428.

[6] F. J. Burpo, E. A. Nagelli, L. A. Morris, J. P. McClure, M. Y. Ryu and J. L. Palmer, *J. Mater. Res.,* 2017, **32**, 4153-4165.

[7] Q. Shi, C. Zhu, H. Zhong, D. Su, N. Li, M. H. Engelhard, H. Xia, Q. Zhang, S. Feng and S. P. Beckman, *ACS Energy Lett.,* 2018, **3**, 2038-2044.

[8] X. Gao, R. J. A. Esteves, L. Nahar, J. Nowaczyk and I. U. Arachchige, *ACS Appl. Mater. Interfaces,* 2016, **8**, 13076-13085.

[9] K. G. Ranmohotti, X. Gao and I. U. Arachchige, *Chem. Mater.,* 2013, **25**, 3528-3534.

[10] C. Zhu, Q. Shi, S. Fu, J. Song, H. Xia, D. Du and Y. Lin, *Adv. Mater.,* 2016, **28**, 8779-8783.

[11] X. Tan, J. Qin, Y. Li, Y. Zeng, G. Zheng, F. Feng and H. Li, *J. Hazard. Mater.,* 2020, **397**, 122786.

[12] N. C. Bigall, A. K. Herrmann, M. Vogel, M. Rose, P. Simon, W. Carrillo-Cabrera, D. Dorfs, S. Kaskel, N. Gaponik and A. Eychmüller, *Angew. Chem. Int. Ed.*, 2009, **48**, 9731-9734.

[13] R. Du, J. Wang, Y. Wang, R. Hübner, X. Fan, I. Senkovska, Y. Hu, S. Kaskel and A. Eychmüller, *Nat. Commun.,* 2020, **11**, 1590.

[14] D. Wen, W. Liu, D. Haubold, C. Zhu, M. Oschatz, M. Holzschuh, A. Wolf, F. Simon, S. Kaskel and A. Eychmüller, *ACS Nano,* 2016, **10**, 2559-2567.

[15] R. Du, Y. Hu, R. Hübner, J.-O. Joswig, X. Fan and A. Eychmüller, *Sci. Adv.,* 2019, **5**, eaaw4590.

[16] F. J. Burpo, E. A. Nagelli, L. A. Morris, J. P. McClure, M. Y. Ryu and J. L. Palmer, *J. Mater. Res.,* 2017, **32**, 4153-4165.

[17] S. Tang, S. Vongehr, Y. Wang, J. Cui, X. Wang and X. Meng, *J. Mater. Chem. A,* 2014, **2**, 3648-3660.

[18] H. Zhao, Y. Yuan, D. Zhang, Y. Qin, Y. Han, H. Li, Z. Wang, S. Li, J. Lai and L. Wang, *ACS Appl. Nano Mater.,* 2021, **4**, 11221-11230.

[19] R. Du, J.-O. Joswig, R. Hübner, L. Zhou, W. Wei, Y. Hu and A. Eychmüller, *Angew. Chem. Int. Ed.,* 2020, **59**, 8293-8300.

[20] R. Du, J.-O Joswig, X. Fan, R. Hübner, D. Spittel, Y. Hu and A. Eychmüller, *Matter*, 2020, **2**, 908-920.

[21] Y. Yuan, H. Zhao, W. Xv, D. Zhang , Z. Wang , H. Li , Y. Qin, S. Li, J. Lai and L. Wang, Chin. Chem. Lett., 2021, https://doi.org/10.1016/j.cclet.2021.09.104